A Supervisory Power Management System for a Hybrid Microgrid with HESS

Srikanth Kotra, *Student Member, IEEE*, Mahesh K. Mishra, *Senior Member, IEEE*

***Abstract*—This paper proposes a supervisory power management system (PMS) for a grid interactive microgrid with a hybrid energy storage system. The key feature of the proposed PMS is reduced number of sensors required to implement the PMS. The PMS considers renewable power variation, grid availability, electricity pricing and changes in local loads. It can detect the operating mode of system without measuring load currents and powers. A single phase voltage source converter transfers real power between DC grid and utility grid besides offering ancillary services such as harmonic mitigation, reactive power support and unity power factor at the point of common coupling. In the proposed system, a better DC link voltage regulation is achieved and the usage of supercapacitors reduces the current stress on battery the battery. The PMS also addresses extreme operating conditions such as load shedding, off-maximum power point tracking operation of PV, elimination of critical oscillation of HESS powers, islanded operation and resynchronization with grid. The performance of the proposed PMS is verified by digital simulation and experimental studies.**

***Index Terms*—Battery, electricity pricing, Power management, hybrid energy storage system, PV power, supercapacitor.**

I. Introduction

THE ever increasing demand for energy efficient appliances is promoting the use of DC appliances in residential and commercial sectors. DC appliances like LED lighting and inverter driven appliances like refrigirators, air conditioners are gaining popularity. At the same time, renewable energy based distribution system is encouraging the use of DC appliances to minimize conversion losses [1]. Therefore, both AC and DC loads will co-exist in renewable-grid integrated distribution system [2]. However, the interconnection of renewable energy sources with grid is a concern for grid operators. When renewable energy sources (RESs) contribute a significant portion of power generation, their irregular and stochastic output variations can bring uncertainties in power system planning and operation. It is reported that many developed countries will supply 78% of their total power consumption using RES [3] by 2050. For example, South Korea plans to produce 12.5% of overall power generation by renewable by 2022. Out of that, 81% is supposed to be generated by the photovoltaic (PV) systems [4]. Therefore, the renewable power generation technology, which consists of PV and storage systems is required to ensure controllability, reliability and stability of overall system.

Manuscript received October 20, 2015; revised March 6, 2016, May 31, 2016 and August 1, 2016; accepted August 16, 2016. This work is supported by the Ministry of Science and Technology, DST India, under the project grant SB/S3/EECE/056/2015.

The authors are with the Department of Electrical Engineering, Indian Institute of Technology Madras, Chennai 600 036, India. (e-mail: ksrikanth225@gmail.com; mahesh@ee.iitm.ac.in).

Generally, hybrid energy storage systems (HESS) like battery and supercapacitor are employed in microgrids to improve reliability and life cycle. The high power density of supercapacitor increases the life cycle of battery [5]–[7]. In a microgrid with HESS, meeting the load demand by maintaining battery and supercapacitor $SoCs$ within limits is an important task due to the uncertainties in RES power. Therefore, the power management system plays a vital role in reliable and continuous operation of the microgrid.

In [8], an EMS is proposed which injects / draws power from grid according to the RES and load power changes. In this work, it is assumed that the microgrid is always connected to the utility grid. Also, the supercapacitor doesn't absorb the transients when the battery reference current is set to zero which increases the rate of change of battery current. This is due to the fact that the EMS changes the battery reference current instantly from zero to reference value during battery mode changes i.e., idle to charging mode / discharging mode and vice-versa. As a result, the battery is forced to respond quickly in spite of having supercapacitor units in the system.

A two stage power control strategy is proposed in [9] to smoothen the power output of a grid connected PV power plant. This technique is purely based on the difference between PV power and grid power. In [4], a unique energy management system is proposed for a grid interactive residential microgrid with energy storage. This method takes the dynamic pricing of grid power into account but does not consider the islanded operation of microgrid which is frequent in residential power sector. In [10] a power balancing technique is proposed which gives better DC link regulation compared to [11]. However, the disturbances in the DC link have to be absorbed by battery which increases the stress on it and thereby decreases the life of battery [12].

In [13]–[15], an integrated control and protection system is proposed for a microgrid. In these systems, the battery voltage rating should be equal to DC link voltage and any disturbance in RES and load should be buffered with battery units. Hence, battery experiences high current stress which reduces it's life span [5]. Also, this method is based on difference between load power and source powers. In [16], a power management method is developed for distributed generators (DG) operating under a common feeder. This method employs communication line to each DG for islanding and grid connection. However, the individual DGs are controlled by measuring difference between source power and load power. In [17], a state machine approach based power management which gives better performance compared to [18]. This method employs fuzzy controller to maintain desired SoC of battery banks and considers 15 distinct operating modes of the microgrid.

This article has been accepted for publication in a future issue of this journal, but has not been fully edited. Content may change prior to final publication. Citation information: DOI 10.1109/TIE.2017.2652345, IEEE Transactions on Industrial Electronics

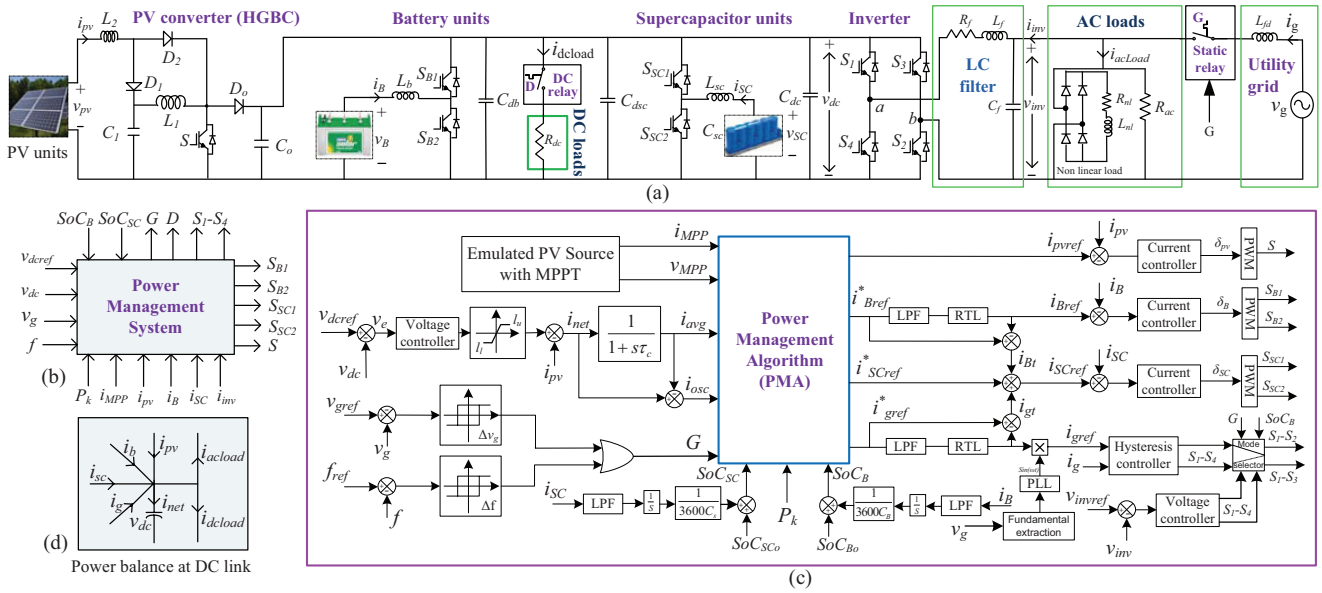

Fig. 1. System configuration and proposed PMS (a) Configuration of grid interactive microgrid with HESS (b) Block diagram of PMS (c) Proposed power management system (d) Power balance at DC link.

However, the off-MPPT mode is not covered in any of the 15 modes. Also, the fixed SoC limits are used in this work.

A rule based control scheme is proposed in [19] to dispatch intermittent renewable energy sources using a BESS. The objective of this control scheme is to maintain the battery SoC with in limits while supplying the power difference. However this scheme does not discuss power balancing when the battery is fully charged / discharged. Also, the DC link voltage regulation is not demonstrated and the local loads are not considered in the system. In [20], a deterministic EMS is proposed for a grid interactive microgrid. This system employs a micro-turbine to support loads in deficit power mode. This system employs communication from each microgrid to the central controller and forecasting of load, PV powers to generate reference quantities. However, It requires measurement of load currents to calculate powers which increases the computation.

A power control strategy is devised in [21] to balance power in a DC microgrid using a battery bank. The main focus of this work is to develop a dedicated local control system to maintain battery SoC and provide an over charge security. The literature in [22]–[25] describes the control strategies for a microgrid which operate the system based on DC link voltage variation. However, the variable DC link voltage affects the performance of DC loads. In [26], a model predictive control (MPC) based power management scheme is proposed for a DC microgrid using HESS which gives a uniform discrete design approach. However, the DC link voltage is assumed to be constant.

According to these research works, the first step in designing an EMS is to identify operating mode of the microgrid. In literature, there are only two techniques available to identify the operating mode of the microgrid. One is based on power difference and the other is based on DC link voltage variation. In this work, we proposed a mode identification technique based on DC link voltage controller output which strictly regulates the DC link voltage. Secondly, there is a need to develop a unified supervisory controller to address every operating mode of the system with minimal components. In this work, we formulated a power management algorithm that addresses all possible operating modes of a microgrid and achieves stable and desirable performance in all modes with reduced number of sensors.

II. System Configuration and Proposed Power Management System

The grid interactive microgrid with HESS considered in this work is shown in Fig. 1(a). The emulated PV source is connected to the common DC link through a high gain boost converter (HGBC) and a single phase inverter is interfacing DC link and utility grid as shown in Fig. 1(a). The battery and supercapacitor units are interfaced with the common DC link through a bidirectional buck-boost converter each as shown in Fig. 1(a). The battery unit supplies/handles average deficit/excess power and the supercapacitor unit absorbs power surges.

The proposed power management system shown in Fig. 1(b), mainly consists of DC link voltage controller, reference current generation from power management algorithm (PMA), battery and grid current smoothing, islanding and re-synchronization detection and converter control scheme as shown in Fig. 1(c).

A. DC link voltage controller

The power balance in the system is achieved by maintaining constant DC link voltage as shown in Fig. 1(d). The voltage control loop generates the reference current (i_{net}) to be injected/drawn into/from the DC link to maintain reference

This article has been accepted for publication in a future issue of this journal, but has not been fully edited. Content may change prior to final publication. Citation information: DOI 10.1109/TIE.2017.2652345, IEEE Transactions on Industrial Electronics

voltage at the DC link as shown in Fig. 1(c).

$$\begin{aligned} v_e(t) &= v_{dcref}(t) - v_{dc}(t) \\ i_{net}(t) &= k_{p1}v_e(t) + k_{i1}\int v_e(t)dt - i_{pv}(t) \end{aligned} \tag{1}$$

where, k_{p1}, k_{i1} are PI controller gains. It is to be noticed that i_{net} is positive when v_e is positive which implies DC link input power is more than output power and vice versa. This nature of i_{net} can be utilized to identify the operating mode of the microgrid. The power balance in the system is,

$$p_l(t) + p_{loss}(t) - p_{pv}(t) = p_{net}(t) \tag{2}$$

where $p_l(t)$ is the sum of AC and DC load powers, i.e., $p_l(t) = p_{dcload} + p_{acload}$. The terms $p_{pv}(t)$ and $p_{loss}(t)$ refer to PV power and power loss in the system and $p_{net}(t)$ is the net power required to regulate the DC link voltage. Here, $p_{net}(t)$ should be supplied by battery or grid along with supercapacitor.

The controller output, $i_{net}(t)$ is derived from the DC link voltage control loop as shown in Fig. 1(a) and is given by (1). The average component, i.e., $i_{avg}(t)$ is extracted by using a low pass filter [24] as,

$$i_{avg}(t) = \frac{1}{1 + s\tau_c} i_{net}(t) \tag{3}$$

where $f_c = 1/\tau_c$ is the cutoff frequency of low pass filter. f_c is selected to be 5 Hz such that the battery / grid currents respond to changes with more than 0.2 s time period. The oscillating component of $i_{net}(t)$ is extracted as follows,

$$i_{osc}(t) = i_{os}(t) + i_{tr}(t) = (1 - \frac{1}{1 + s\tau_c})i_{net}(t). \tag{4}$$

The PMA allocates $i_{osc}(t)$ to supercapacitor and $i_{avg}(t)$ to utility grid / battery / PV depending on $i_{avg}(t)$, availability of grid and status of battery SoC. Effectively, $i_{avg}(t)$ decides the operating mode of microgrid.

B. Power Management Algorithm (PMA)

The PMA decides the operating mode of the system based on $i_{avg}(t)$ as shown in Fig. 2. The PMA is formulated with following operational objectives. (i) to identify the operating mode of the system and make decisions based on $i_{avg}(t)$, (ii) to achieve power balance in every operating mode, (iii) to maintain Battery and supercapacitor SoCs within limits and to eliminate current oscillation of HESS at the verge of SoCs, (iv) to supply average power by battery only if the system is islanded, (v) to supply oscillating and transient peak powers by supercapacitor only, (vi) to minimize/maximize power drawn/supplied from/to grid during peak pricing and (vii) to provide minimum backup for critical loads in islanded mode.

There are three possible operating modes of the system, namely (i) Deficit power mode (DPM) (ii) Floating power mode (FPM) (iii) Excess power mode (EPM). FPM is merged with DPM as the HESS can be charged from grid in both modes. Hence, there are two effective operating modes as shown in Fig. 2.

In both modes of operation, there are three sub-modes based on the availability of grid (G) and peak pricing status (P_k) as shown in Fig. 2. They are (i) Peak pricing mode (ii) Off-peak pricing mode (iii) Islanded mode. In each sub-mode, SoC_B and SoC_{SC} are monitored and maintained within limits. If grid power pricing is high then P_k is set to high (1), else set to low (0). Similarly, when the system is connected to grid then G is set to high (1), else set to low (0). A rule based control [27] is developed to implement the PMA. The algorithm is initialized with battery SoC lower limit B_L and upper limit B_U are set to 0.25 and 0.9 respectively and supercapacitor SoC lower limit S_L and upper limit S_U are set to 0.2 and 0.9 respectively.

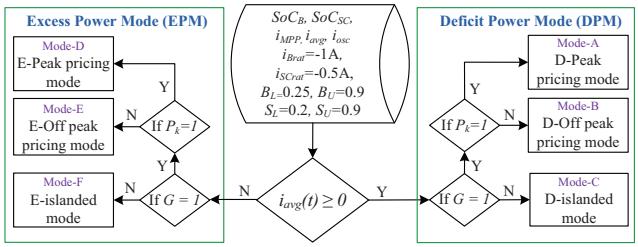

Fig. 2. Simplified block diagram of PMA.

1) Deficit power mode: ($i_{avg} \geq 0$)(Cases:1-14)

In DPM, the average current $(i_{avg}(t))$ is greater than or equal to zero and there are three sub-modes explained as following.

Mode A: *D-peak pricing mode (Cases:1-4)*

In this mode, grid is *on* and peak pricing is enabled i.e., $G = 1, P_k = 1$. Therefore, minimum amount of power is drawn from the grid. The deficit power is drawn from grid while charging battery and supercapacitor upto 50% of their capacity by updating $B_L = 0.5$ and $S_L = 0.5$. There are four possible cases depending on SoC_B and SoC_{SC} as shown in Fig. 3. In those four cases, battery and supercapacitor are charged if their SoCs are less than their respective *lower limits*, else battery will be idle and supercapacitor supplies transient and oscillating powers as shown in Fig. 3.

Mode B: *D-off peak pricing mode (Cases:5-8)*

In this mode, grid is *on* and peak pricing is disabled i.e., $G = 1, P_k = 0$. As the grid power pricing is less, the deficit power is drawn from grid while charging battery and supercapacitor upto 90% of their capacity by updating $B_U = 0.9$ and $S_U = 0.9$ as shown in Fig. 3.

Mode C: *D-islanded mode (Cases:9-14)*

In this mode, grid is *off* i.e., $G = 0$. Therefore, the deficit power is to be supplied by HESS or proportionate load should be shed. There are three branches (a), (b)& (c) in this mode as shown in Fig. 3.

(a) *(Cases:9-10)*: If SoC_B is more than 0.5 then both DC and AC loads are supplied power from battery and inverter is operated in voltage control mode (VCM) to supply power to AC loads at rated voltage and frequency. The supercapacitor supplies oscillating power while regulating its SoC.

(b) *(Cases:11-12)*: If SoC_B is between B_L and 0.5 then DC loads are supplied and AC loads are turned off by resetting inverter pulses.

This article has been accepted for publication in a future issue of this journal, but has not been fully edited. Content may change prior to final publication. Citation information: DOI 10.1109/TIE.2017.2652345, IEEE Transactions on Industrial Electronics

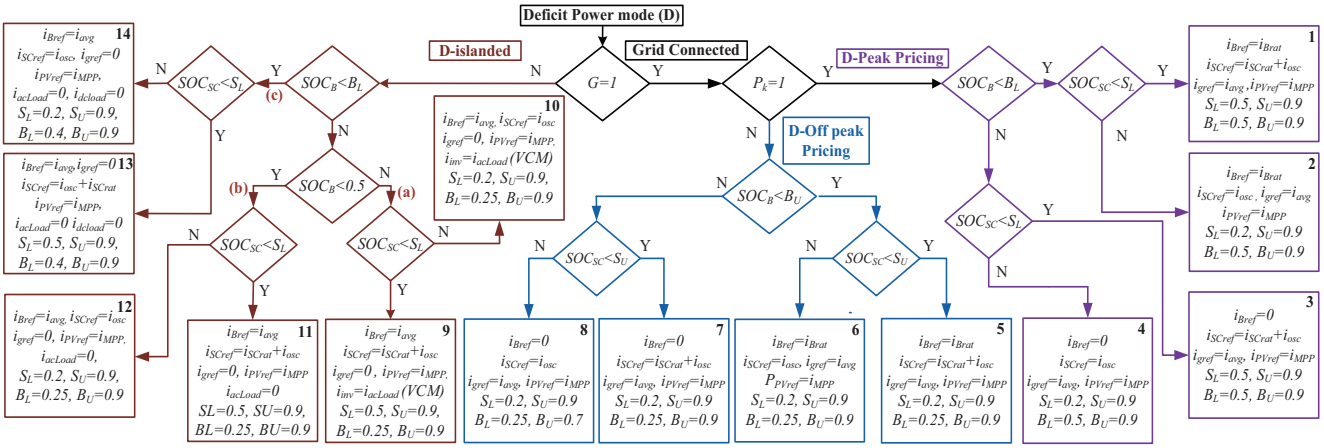

Fig. 3. Flowchart of deficit power mode.

(c) *(Cases:13-14)*: If SOC_B is less than B_L both AC and DC loads are turned off and the total power from PV is fed to the battery.

In cases 11-14, the system may enter into excess mode due to load shedding. So, the same cases are re-addressed in E-islanded mode as shown in Fig. 4.

2) Excess power mode: (i_{avg}<0) *(Cases:15-28)*

In EPM, the average current, $i_{avg}(t)$ is less than zero and there are three sub-modes explained as following.

Mode D: *E-peak pricing mode (Cases:15-18)*

In this mode, grid is *on* and peak pricing is enabled i.e., $G = 1, P_k = 1$. Therefore, maximum possible amount of excess power is injected into the grid by limiting battery and supercapacitor charging up to 50% of their capacity by updating $B_L = 0.5$ and $S_L = 0.5$. As the power is injected into the grid, it is referred as *grid injecting mode*.

Mode E: *E-off peak pricing mode (Cases:19-22)*

In this mode, grid is *on* and peak pricing is disabled i.e., $G = 1, P_k = 0$. Therefore, the excess power is preferred to charge battery and supercapacitor upto 90% of their capacity by updating $B_U = 0.9$ and $S_U = 0.9$ as the pricing of power injected into the grid is less. Once the battery and supercapacitor are fully charged, the excess power is injected into grid.

Mode F: *E-islanded mode (Cases:23-28)*

In this mode, grid is *off* i.e., $G = 0$. Therefore, the excess power has to be absorbed by HESS or the PV power should be controlled such that it is equal to load power. There are four branches in this mode as shown in Fig. 4.

(d) *(Cases:23-24)*: In this mode, SoC_B is more than 0.5. Therefore, both AC and DC loads are supplied from PV and inverter is operated in voltage control mode (VCM) to maintain rated voltage and frequency on ac side. If any excess power is available, it is utilized to charge battery and supercapacitor.

(e) *(Cases:25-26)*: In this mode SoC_B is in between B_L and 0.5. Therefore, DC loads are supplied and AC loads are turned off and the excess power is used to charge battery.

(f) *(Cases:27-28)*: In this mode SOC_B is more than B_U. Therefore, PV is operated in *off-MPPT mode*. In other words, PV is operated in voltage control mode (VCM).

(g) *(Cases:11-14)*: If SOC_B is less than B_L then deficit mode Cases 11-14 are executed until SoC_B increases beyond B_L.

C. Battery and Grid Current Smoothing

The battery and grid reference currents generated by PMA causes battery and grid to undergo current stress during mode changes. Therefore, to reduce the rate of change of battery current and to achieve a seamless mode transfer of grid from grid supply mode to grid injecting mode and grid connected mode to islanded mode and vice versa, the sudden changes in $i_{Bref}(t)$ and $i_{gref}(t)$ are allocated to the supercapacitor as given by (5),

$$i_{SCref}(t) = i_{osc}(t) + i_{Bt}(t) + i_{gt}(t) \tag{5}$$

where $i_{SCref}(t)$ is the supercapacitor reference current, $i_{osc}(t)$ is the net sum of oscillating and transient currents and $i_{Bt}(t)$, $i_{gt}(t)$ are battery and grid transient currents respectively.

D. Smooth islanding and re-synchronization

In the proposed system, the microgrid islanding is detected by over / under voltage / frequency (OUV/OUF) method [28]. The microgrid is islanded if the grid voltage deviates from 0.88-1.1 p.u or the frequency deviates from 49.3-50.5 Hz complying with the IEEE Std. 1547. When the microgrid is islanded, the grid status G is updated to 0 and the PMA sends a command signal to the grid relay and the inverter is operated in voltage control mode (VCM). Once the grid voltage and frequency are restored, the relay is closed at zero crossing of grid voltage and the inverter is operated in current control mode (CCM). Accurate grid synchronization is achieved by generating grid current reference from grid voltage using PLL. An indirect current control strategy is employed in this work which gives the feature of unity power factor and sinusoidal grid current [8].

III. Stability Analysis of Proposed Microgrid

The stability analysis of proposed system is done by considering $5ms$ of communication delay for all converters. The

This article has been accepted for publication in a future issue of this journal, but has not been fully edited. Content may change prior to final publication. Citation information: DOI 10.1109/TIE.2017.2652345, IEEE Transactions on Industrial Electronics

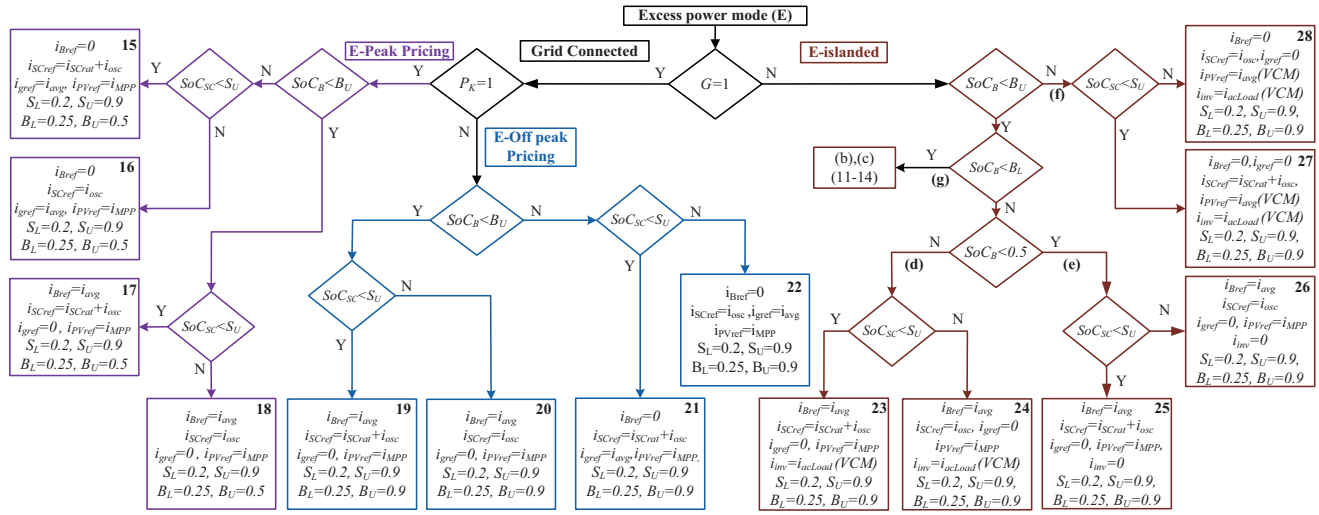

Fig. 4. Flowchart of excess power mode

power balance and stability in the system are monitored by regulating the DC link voltage. The DC link voltage controller remains same in all control strategies. The DC link voltage controller is designed such that it provides the desired phase margin and gain margin with any of the three converters i.e battery or PV or grid converters after considering communication delays.

There are mainly three control strategies in the proposed PMS. They are,

1. Grid connected mode- grid maintains v_{dc} in this mode.
2. Islanded mode- battery maintains v_{dc} in this mode.
3. Off-MPPT Mode- PV maintains v_{dc} in this mode.

The control block diagram in grid connected mode is shown in Fig. 5(a) and the small signal model is derived as shown in Fig. 5(b).

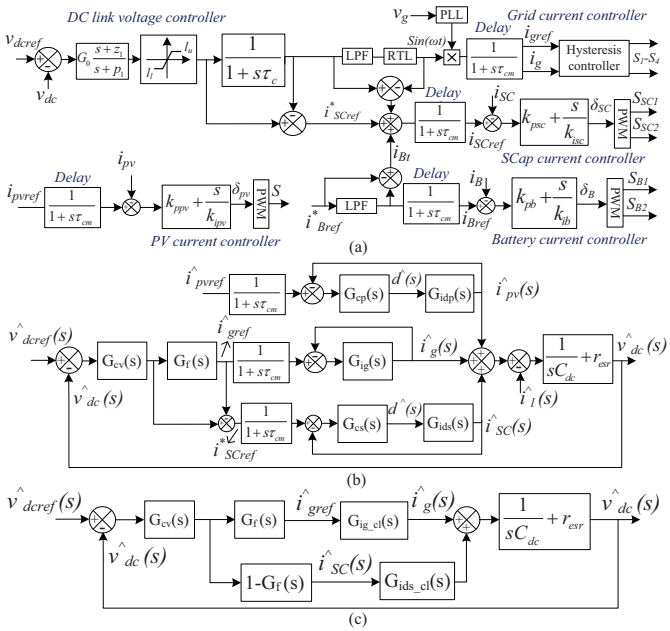

Fig. 5. Control block in grid connected mode (a) Control block diagram (b) Small signal model (c) Simplified small signal model

To derive the loop gain from reference voltage to output voltage, other disturbances are made zero and the simplified model shown in Fig. 5(c) is obtained. Where $G_{cv}(s)$, $G_f(s)$, $G_{ig}(s)$, $G_{cs}(s)$, $G_{ids}(s)$, $G_{cp}(s)$ and $G_{idp}(s)$ are transfer functions of DC link voltage controller, low pass filter, grid converter, supercapacitor current controller, supercapacitor converter in current control mode, PV current controller and PV converter in current control mode respectively.

The loop gain of the simplified small signal model is,

$$GH(s) = G_{cv}(s)[G_f(s)G_{ig\_cl}(s) + (1 - G_f(s))G_{idsc\_cl}] \times [\frac{1}{sC_{dc\_total}} + R_{esr}] \quad (6)$$

where, $G_{cv}(s) = G_0(\frac{s+z_1}{s+p_1})$, $G_f(s) = \frac{1}{1+s\tau}$, $G_{cs}(s) = k_{ps} + \frac{k_{is}}{s}$, $G_{ids}(s) = \frac{s(C_{dc\_total}V_{dc})+2D^{'}I_{Lsc}}{s^2L_{sc}C_{dc\_total}+s\frac{L_{sc}}{R_L}+D'^2}$ and $G_{idsc\_cl}(s) = \frac{G_{cs}(s)G_{ids}(s)}{1+G_{cs}(s)G_{ids}(s)} * \frac{1}{1+s\tau_c}$ and G_0= 347.5542, z_1= 0.06779, p_1= 27.2018, τ= 0.7, k_{pgi}= 0.5, k_1= 0.5, k_3= 0.5, k_{ps}= 0.4, k_{is}= 0.1, L_{sc}= 5 mH, R_L= 100 , $D^{'}$= 0.48, I_{Lsc}= 5A and C_{dc_total}= 2860 μF.

With these design parameters the bode plot of the system is shown in Fig. 6. It can be observed that the grid current control loop has infinity gain margin and a phase margin of $47.1°$ and DC bus voltage is stable for changes in grid reference current. This also implies that the DC bus voltage is stable when the system changes its mode form islanded to grid connected.

Similarly, the control block diagram, small signal model and simplified small signal model for islanded mode are shown in Fig. 7.

The loop gain of the control loop in islanded mode is given by,

$$GH(s) = G_{cv}(s)[G_f(s)G_{idb\_cl}(s) + (1 - G_f(s))G_{idsc\_cl}] \times [\frac{1}{sC_{dc\_total}} + R_{esr}] \quad (7)$$

where, $G_{cb}(s) = k_{pb} + \frac{k_{ib}}{s}$, and k_{pb}=0.01, k_{ib}=0.5, L_b=5 mH, R_L=100, $D^{'}$=0.6, I_{Lb}=10A, $G_{idb\_cl}(s) = \frac{G_{cs}(s)G_{ids}(s)}{1+G_{cs}(s)G_{ids}(s)}$

This article has been accepted for publication in a future issue of this journal, but has not been fully edited. Content may change prior to final publication. Citation information: DOI 10.1109/TIE.2017.2652345, IEEE Transactions on Industrial Electronics

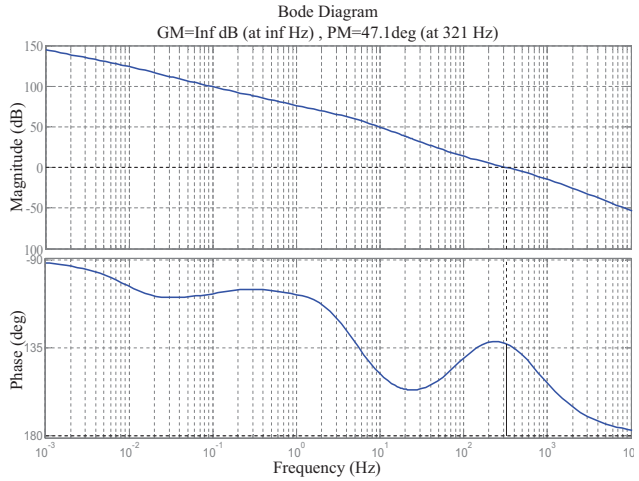

Fig. 6. Bode plot of control loop gain in grid connected mode

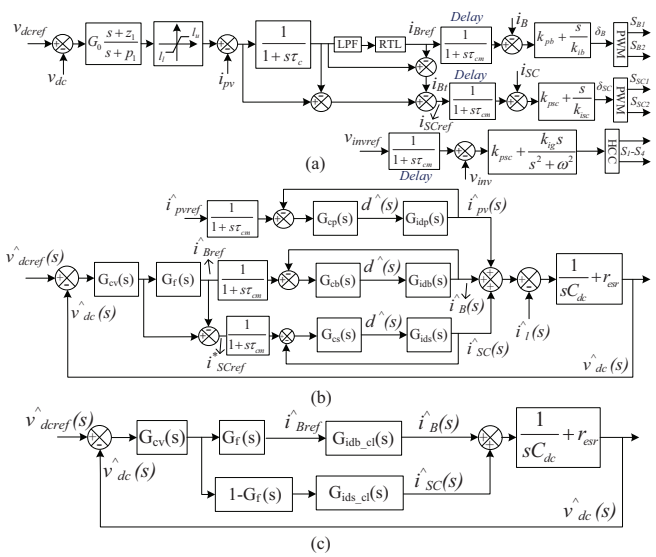

Fig. 7. Control block in islanded mode (a) Control block diagram (b) Small signal model (c) Simplified small signal model

$$G_{idb}(s) = \frac{s(C_{dc\_total}V_{dc})+2D^{'}I_{Lb}}{s^2L_bC_{dc\_total}+s\frac{L_b}{R_L}+D'^2}.$$

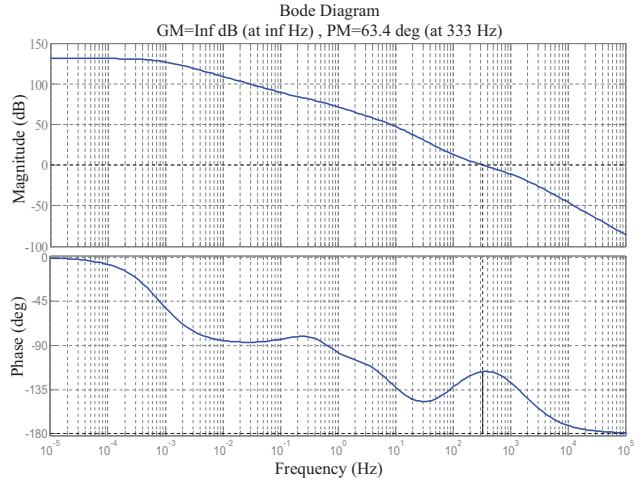

Fig. 8. Bode plot of control loop gain in islanded mode

The only change in loop gain of islanded mode to grid connected mode is that the closed loop transfer function of grid converter is replaced by that of battery converter. With the above design parameters the Bode plot of the system is shown in Fig. 8. With battery converter the phase margin is found to be 63.4°. It can be observed that the phase margin of loop gain with grid converter and battery converter is almost same due to the fact that the closed loop transfer function of the battery converter is unity till the cross over frequency which does not affect the gain cross over frequency. Therefore the system is stable in islanded mode. This also implies that the DC grid is stable when the system is islanded from utility grid. Similarly, the stability in Off-MPPT mode is verified.

TABLE I
SYSTEM PARAMETERS

Parameter	Values
Battery Pack: Ah Capacity, Terminal voltage	26 Ah, 60 V
Supercapacitor Pack: C, V_{rated}, I_{peak}	19.33 F, 48 V, 200 A
Battery converter: L_b, C_{db}	5 mH, 220 μF
Supercapacitor converter: L_{sc}, C_{dsc}	5 mH, 220 μF
HGBC parameters: L_1, L_2, C_0	5 mH, 5 mH, 220 μF
VSC Parameters: C_{dc}, C_f L_f, R_f	2200 μF, 10 μF 10 mH, 0.1 Ω
AC and DC loads: R_{dc}, R_{ac} R_{nl}, L_{nl}	100 Ω, 50 Ω 50 Ω, 50 mH
Utility and DC link voltage: V_g & V_{dc}	50 V & 100 V

IV. SIMULATION RESULTS

The proposed system is modeled using Matlab/Simulink tool and the efficacy of proposed PMS is verified in all modes of operation by changing grid availability, peak pricing, HESS SoCs and maximum power point current of PV as shown in Fig. 9(a)-(c). The simulation is carried out for a duration of 40 s to test all the 28 modes of operation as explained in the following section and tabulated in Table II.

A. Deficit power mode (Cases:1-14)

1) D-Peak pricing mode (Cases:1-4): The system is started at t= 0 s with utility grid is *on* state, peak pricing is enabled, i_{MPP} is set to 1 A and $SoC_B < B_L$ and $SoC_{SC} < S_L$. At t= 0 s, supercapacitor supplies peak current until the battery reaches steady state and DC link voltage settles at rated value. In case 1, i.e., 0-2 s, grid supplies average deficit power and battery, supercapacitor units are charged with rated currents 1 A and 0.5 A respectively as their SoCs are less than the lower limits and both B_L, S_L are updated to 0.5. From Fig. 9(c)-(d), it can be observed that at t =1 s, the battery and supercapacitor keep on charging though SoC_B and SoC_{SC} are increased to 0.4 and the battery / supercapacitor stops charging as soon as SoC_B/SoC_{SC} crosses the new lower limit (B_L/S_L). This eliminates the critical oscillation of HESS powers at SoC limits.

2) D-Off peak pricing mode (Cases:5-8): At t= 6 s, peak pricing is disabled and battery is allowed to charge up to the full capacity from grid. In case 5, t= 6-8 s, SoC_B and SoC_{SC} are set lower than B_U and S_U respectively. This makes the battery and supercapacitor to charge with rated current until

This article has been accepted for publication in a future issue of this journal, but has not been fully edited. Content may change prior to final publication. Citation information: DOI 10.1109/TIE.2017.2652345, IEEE Transactions on Industrial Electronics

TABLE II
OPERATING MODES OF THE SYSTEM

Cases	*Sim*	*Exp*	P_{pv}	*Grid*	P_k	SoC_B	SoC_{SC}	i_B	i_{SC}	i_{inv}	i_{pv}	B_L	B_U
Case 1	0--1	t_1-t_2	<P_L	*on*	1	0.2	0.15	i_{Brat}	$i_{SCrat}+i_{osc}$	*CCM*	i_{MPP}	0.5	0.9
	1--2	t_2-t_3	<P_L	*on*	1	0.4	0.4	i_{Brat}	$i_{SCrat}+i_{osc}$	*CCM*	i_{MPP}	0.5	0.9
Case 2	2--3	t_3-t_4	<P_L	*on*	1	0.4	0.6	i_{Brat}	i_{osc}	*CCM*	i_{MPP}	0.5	0.9
Case 3	3--4	t_6-t_7	<P_L	*on*	1	0.6	0.15	0	$i_{SCrat}+i_{osc}$	*CCM*	i_{MPP}	0.5	0.9
	4--5	t_6-t_7	<P_L	*on*	1	0.6	0.4	0	$i_{SCrat}+i_{osc}$	*CCM*	i_{MPP}	0.5	0.9
Case 4	5--6	t_4-t_5	<P_L	*on*	1	0.6	0.6	0	i_{osc}	*CCM*	i_{MPP}	0.5	0.9
Case 5	6--8	t_8-t_9	<P_L	*on*	0	0.7	0.7	i_{Brat}	$i_{SCrat}+i_{osc}$	*CCM*	i_{MPP}	0.25	0.9
Case 6	8--9	t_9-t_{10}	<P_L	*on*	0	0.7	0.95	i_{Brat}	i_{osc}	*CCM*	i_{MPP}	0.25	0.9
Case 7	9--11		<P_L	*on*	0	0.95	0.7	0	$i_{SCrat}+i_{osc}$	*CCM*	i_{MPP}	0.25	0.9
Case 8	11--12	t_1-t_8	<P_L	*on*	0	0.95	0.95	0	i_{osc}	*CCM*	i_{MPP}	0.25	0.9
Case 9	12--14	t_1-t_9	<P_L	*off*	0	0.7	0.15	i_{avg}	$i_{SCrat}+i_{osc}$	*VCM*	i_{MPP}	0.25	0.5
Case 10	14--15	t_{12}-t_{13}	<P_L	*off*	0	0.7	0.6	i_{avg}	i_{osc}	*VCM*	i_{MPP}	0.25	0.9
Case 11	15--16		<P_L	*off*	0	0.45	0.15	i_{avg}	$i_{SCrat}+i_{osc}$	0	i_{MPP}	0.25	0.9
Case 12	16--17	t_{13}-t_{14}	<P_L	*off*	0	0.45	0.6	i_{avg}	i_{osc}	0	i_{MPP}	0.25	0.9
Case 13	17--19		<P_L	*off*	0	0.2	0.15	i_{avg}	$i_{SCrat}+i_{osc}$	0	i_{MPP}	0.4	0.9
Case 14	19--20	t_{15}-t_{16}	<P_L	*off*	0	0.2	0.6	i_{avg}	i_{osc}	0	i_{MPP}	0.4	0.9
Case 4	20-21		<P_L	*on*	1	0.6	0.7	0	i_{osc}	*CCM*	i_{MPP}	0.5	0.9
Case 15	21--23		>P_L	*on*	1	0.6	0.7	0	$i_{SCrat}+i_{osc}$	*CCM*	i_{MPP}	0.25	0.5
Case 16	23--24	t_{17}-t_{18}	>P_L	*on*	1	0.6	0.95	0	i_{osc}	*CCM*	i_{MPP}	0.25	0.5
Case 17	24--25	t_{16}-t_{17}	>P_L	*on*	1	0.4	0.7	i_{avg}	$i_{SCrat}+i_{osc}$	*CCM*	i_{MPP}	0.25	0.5
Case 18	25--26		>P_L	*on*	1	0.4	0.95	i_{avg}	i_{osc}	*CCM*	i_{MPP}	0.25	0.5
Case 19	26--28		>P_L	*on*	0	0.7	0.7	i_{avg}	$i_{SCrat}+i_{osc}$	*CCM*	i_{MPP}	0.25	0.9
Case 20	28--29	t_{18}-t_{19}	>P_L	*on*	0	0.7	0.95	i_{avg}	i_{osc}	*CCM*	i_{MPP}	0.25	0.9
Case 21	29--31		>P_L	*on*	0	0.95	0.7	0	$i_{SCrat}+i_{osc}$	*CCM*	i_{MPP}	0.25	0.9
Case 22	31--32	t_{19}-t_{20}	>P_L	*on*	0	0.95	0.95	0	i_{osc}	*CCM*	i_{MPP}	0.25	0.9
Case 23	32--34		>P_L	*off*	0	0.7	0.7	i_{avg}	$i_{SCrat}+i_{osc}$	*VCM*	i_{MPP}	0.25	0.9
Case 24	34--35	t_{21}-t_{22}	>P_L	*off*	0	0.7	0.95	i_{avg}	i_{osc}	*VCM*	i_{MPP}	0.25	0.9
Case 25	35--36		>P_L	*off*	0	0.45	0.7	i_{avg}	$i_{SCrat}+i_{osc}$	0	i_{MPP}	0.25	0.9
Case 26	36--37	t_{20}-t_{21}	>P_L	*off*	0	0.45	0.95	i_{avg}	i_{osc}	0	i_{MPP}	0.25	0.9
Case 27	37--38		>P_L	*off*	0	0.95	0.7	0	$i_{SCrat}+i_{osc}$	*VCM*	*VCM*	0.25	0.9
Case 28	38--40	t_{22}-t_{25}	>P_L	*off*	0	0.95	0.95	0	i_{osc}	*VCM*	*VCM*	0.25	0.9
dclc		t_{23}-t_{24}	>P_L	*off*	0	0.95	0.95	0	i_{osc}	*VCM*	*VCM*	0.25	0.9
aclc	38.25--40	t_{24}-t_{25}	>P_L	*off*	0	0.95	0.95	0	i_{osc}	*VCM*	*VCM*	0.25	0.9

DPM	AC load shedding	Grid injecting	Grid mode transfer	dclc-DC load change
EPM	AC and DC load shedding	*Off-MPPT operation of PV*		aclc-AC load change

their SoCs reach the upper limit B_U and S_U respectively. Similarly, cases 6-8 can be observed from t=8-12 s in Fig. 9 and Table II.

3) D-islanded mode (Cases:9-14): At t=12 s, the grid goes off. Therefore, the system enters into islanded mode as shown in Fig. 9(e). In Cases 9 and 10, battery supplies the deficit power and inverter is operated in voltage control mode (VCM) to supply power to AC loads. For case 11 and 12, SoC_B is less than 0.5. Therefore, AC loads are shed by resetting the inverter pulses and battery supplies/absorbs deficit/excess power. For cases 13 and 14, SoC_B is made less than B_L and PV power is very low and not enough to supply loads. Therefore, both AC and DC loads are shed by PMA as shown in Fig. 9(g)-(h) and battery is charged .

B. Excess power mode (Cases:15-28)

E-peak pricing mode i.e., cases 15-18 and E-off peak pricing mode i.e., cases 19-22 are illustrated in Fig. 9 and given in Table II. At t=21 s, i_{MPP} is increased from 4 A to 6 A as shown in Fig. 9(b) which makes the system to enter into grid injecting mode. Cases 23-26 are verified and tabulated in Table II. In E-islanded mode, at t=32 s the grid goes off i.e., the system enters into islanded mode and the corresponding cases 23-26 are tabulated in Table II. At t=37 s, both SoC_B and SoC_{SC} are set higher than their upper limits B_U and S_U

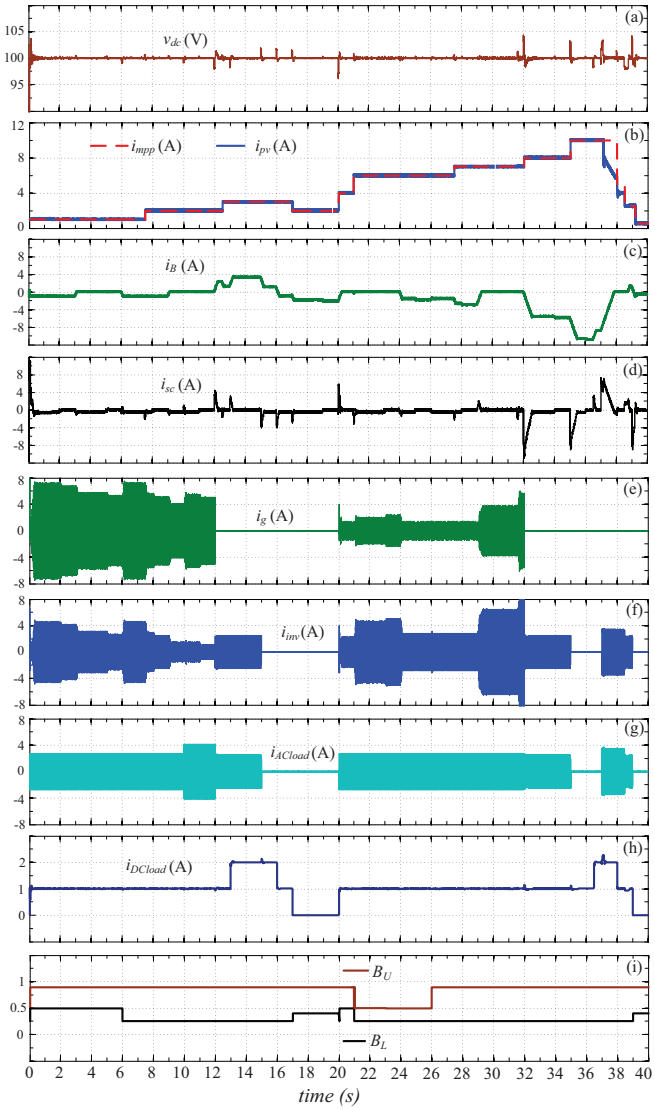

Fig. 9. Performance of microgrid with proposed PMS (a) DC bus voltage (b) MPPT reference current and PV current (c) Battery current (d) Supercapacitor current (e) Grid current (f) Inverter current (g) AC load current (h) DC load currents (i) Battery upper and lower SoC limits

respectively. As the system is in islanded mode and HESS is fully charged, PV is operated in *off-MPPT mode* till t=38.5 s as shown in Fig. 9(b). *Off-MPPT* is achieved by changing PV reference current i_{PVref} from i_{MPP} to i_{avg}.

V. EXPERIMENTAL RESULTS

The experimental setup of hybrid microgrid with HESS is shown in Fig. 10. It consists of an emulated PV source, simulated utility grid, battery unit, supercapacitor unit, HGBC, two bidirectional converters, DC and AC loads and a single phase VSC. The proposed PMS is implemented in real time using dSPACE 1104 control board.

The parameters used for experimental study are given in Table I. There are 28 cases grouped into 6 modes as shown in Fig. 2. Only 18 cases are shown in the experimental results and rest 10 cases are omitted. Because, in those cases, only the supercapacitor goes into charging mode and rest of the

This article has been accepted for publication in a future issue of this journal, but has not been fully edited. Content may change prior to final publication. Citation information: DOI 10.1109/TIE.2017.2652345, IEEE Transactions on Industrial Electronics

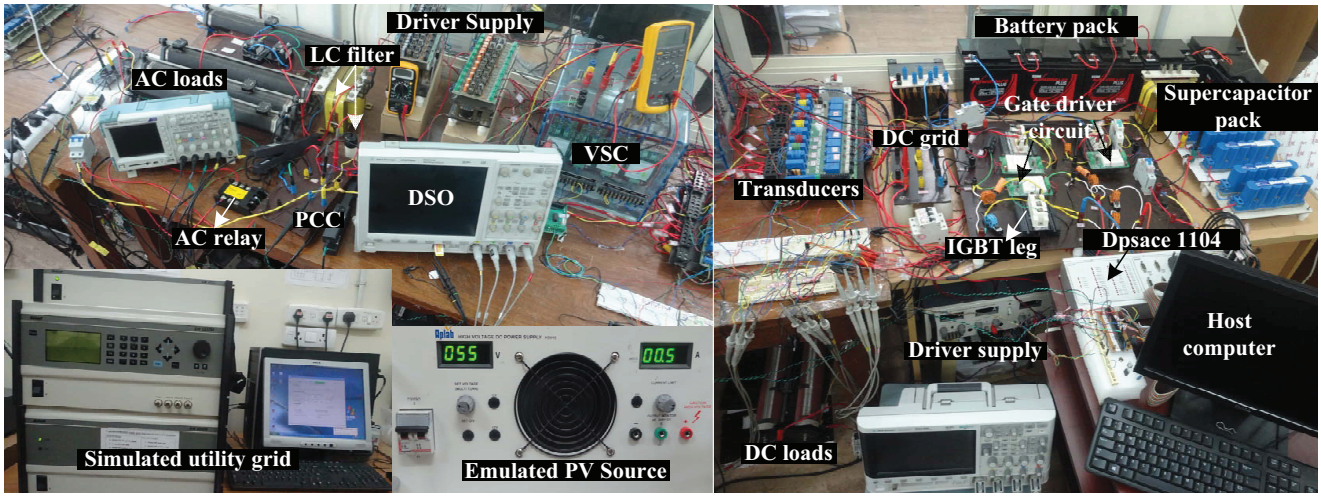

Fig. 10. Experimental setup of grid interactive microgrid with HESS.

system operation remains same as its preceding or following case.

The PMS is initiated at t_1 instant with battery and supercapacitor SoCs less than their lower limits of 0.25 and 0.2 respectively. Therefore, both battery and supercapacitor charge from grid as shown in Fig.11 until their SoCs reach the updated lower limit of 0.5. Similarly, all operating modes are illustrated in Fig. 11 and tabulated in Table II. Few important modes are discussed in the following section.

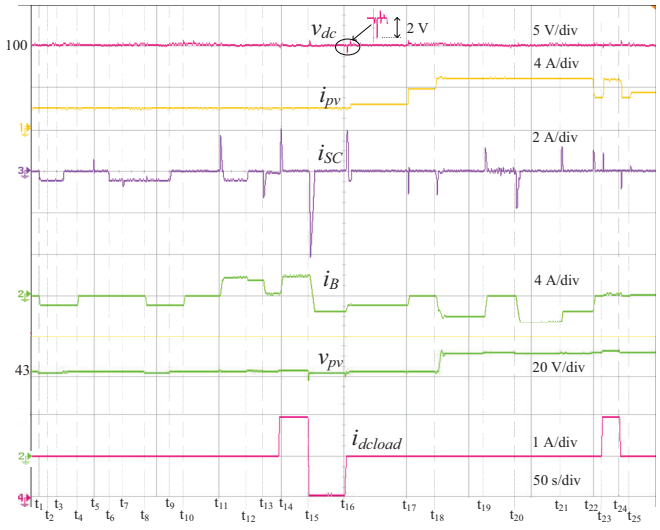

Fig. 11. Experimental results of proposed PMS: DC link voltage, PV current, supercapacitor current, battery current, PV voltage, DC load current.

In Mode C i.e., deficit islanded mode, at t_{11} instant, the grid voltage is decreased to zero as shown in Fig. 12 and 13(a). The PMA detects the disturbance and islands the microgrid by activating the grid relay. As the SoC_B is more than 0.5, AC loads are supplied power by restoring voltage on AC side of VSC as shown in 13(a). The islanding of microgrid is achieved in 20 ms which can be observed from Fig. 13(a). This value satisfies the requirement of 0.16 s given in IEEE Std. 1547. At t_{16} instant, the utility grid voltage is restored. The PMA

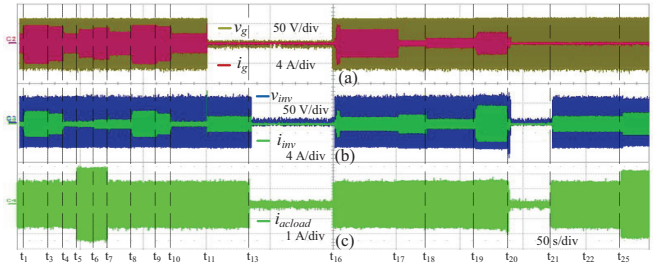

Fig. 12. Experimental results of proposed PMS: (a) Grid voltage and grid current (b) Inverter voltage and inverter current (c) AC load current.

detects the grid voltage restoration and closes the relay in 0.21 s as shown in Fig. 13(b). It can be noticed that the AC loads are off from $t_{13} - t_{16}$ as SoC_B is less than 0.5 in islanded mode.

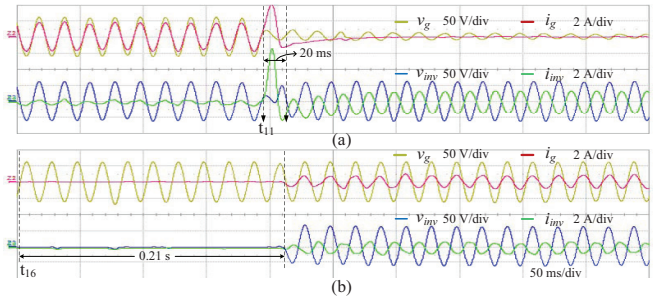

Fig. 13. Experimental results showing islanding and re-synchronization (a) Zoomed view of Fig. 12 at t_{11} instant (b) Zoomed view of Fig. 12 at t_{16} instant.

In Mode F i.e., excess islanded mode, at t_{22} instant both SoC_B and SoC_{SC} are set to 0.95 which is higher than their upper limits (0.9) and i_{MPP} is increased to 6 A. This forces the system to operate in *off-MPPT mode* and i_{pv} decreases to 3 A as illustrated in Fig. 14. It can be noticed that the DC load is increased by 100% at t_{23} instant, due to which i_{pv} increases from 3A to 5A as shown in Fig. 14. At t_{23} instant the DC load is decreased to 50%, due to which i_{pv} decreases from 5A to 3A as shown in Fig. 14.

It can be noticed that due to battery current smoothing, the

This article has been accepted for publication in a future issue of this journal, but has not been fully edited. Content may change prior to final publication. Citation information: DOI 10.1109/TIE.2017.2652345, IEEE Transactions on Industrial Electronics

rate of change of battery current and peak overshoot of v_{dc} are decreased to 0.93A/s and 2V respectively compared to that of 1.8 A/s and 5.2V in [8].

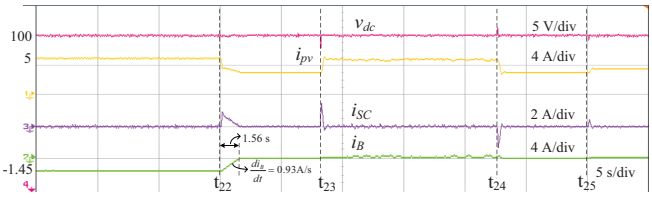

Fig. 14. Experimental results showing *off-MPP* operation: Zoomed view of v_{dc}, i_{pv}, i_{SC} and i_B from Fig. 11.

In grid connected mode, at t_{26} instant the PV current is increased from 0.5 A to 4.5 A as shown in Fig. 15(a) by keeping SoC_B and SoC_{SC} higher than their upper limits. This forces the system to enter into excess power mode. As battery and supercapacitor are fully charged, the excess power is injected into the grid as shown in Fig. 15(a). The sudden increase in PV power is absorbed by supercapacitor and the grid current i_g changes from 3 A in phase with grid voltage v_g to 0 A and increases to 3 A in out of phase with grid voltage v_g in 0.35 s as shown in Fig. 15(a). This seamless phase reversal of i_g eliminates the oscillations during mode transfer of grid.

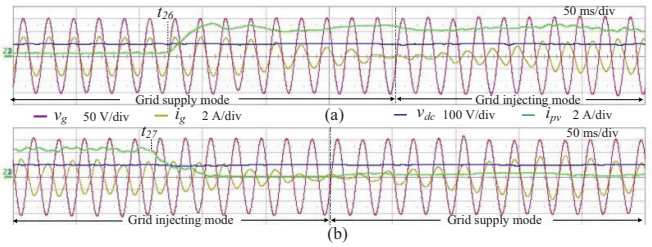

Fig. 15. Experimental results showing seamless mode transfer of grid: v_{dc}, i_{pv}, v_g and i_g during (a) mode transfer from grid supply mode to grid injecting mode (b) mode transfer from grid injecting mode to grid supply mode.

Similarly, mode transfer from grid injecting mode to grid supply mode is illustrated in Fig. 15(b). It can also be noticed that i_g is sinusoidal and in phase with v_g in grid supply mode and in exactly out of phase with v_g in grid injecting mode and the THD of i_g is found to be 3.6% which illustrates the power quality features of proposed PMS.

TABLE III
PERFORMANCE COMPARISON BETWEEN VARIOUS PMSS

Parameters	Scheme I	Scheme II	Proposed PMS
DC link voltage(v_{dc})			
$t_s(s)$	0.15	0.25	0.2
Mp (%)	10	5.3	2
$e_{ss}(V)$	4	0.1	0.1
Battery current di_B/dt	25 A/s	1.4 A/s	0.93 A/s
%THD	5.2%	4.2%	3.6%

In this table, t_s, Mp, e_{ss}, and di_B/dt represent settling time, peak overshoot, steady state error of v_{dc} and rate of change of battery current respectively.

The performance of proposed PMS is compared with PMS given in [10] (scheme I) and [8] (scheme II) and key observations are given in Table III. The proposed method has superior performance compared to scheme-I and scheme-II.

VI. CONCLUSION

A unified power management scheme is proposed for a grid interactive hybrid microgrid with HESS. The new method of identifying microgrid operating mode is proposed and verified in all possible operating modes. The formulated PMS addresses the possible operating modes of the microgrid and achieves stable and desirable performance. It is shown that the proposed PMS ensures reliable and continuous power supply to the local loads and enables the bidirectional real power transfer between the microgrid and the utility grid while improving the power quality aspects at the PCC. Various features like fast DC link voltage regulation, reduced battery current stresses, *Off-MPPT* operation are illustrated. The proposed PMS achieves seamless mode transfer using supercapacitor units. The power quality at the point of common coupling is maintained as per the grid standards. Also, the proposed PMS does not require forecasting of weather and measurement load currents / powers, which reduces the complexity and number of sensors.

REFERENCES

[1] O. Lucia, I. Cvetkovic, H. Sarnago, D. Boroyevich, P. Mattavelli, and F. Lee, "Design of home appliances for a dc-based nanogrid system: An induction range study case," *IEEE J. Emerg. Sel.Topics Power Electron.*, vol. 1, no. 4, pp. 315–326, Dec 2013.

[2] F. Nejabatkhah and Y. W. Li, "Overview of power management strategies of hybrid ac/dc microgrid," *IEEE Trans. Power Electron.*, vol. 30, no. 12, pp. 7072–7089, Dec 2015.

[3] P. Denholm, R. Margolis, T. Mai, G. Brinkman, E. Drury, M. Hand, and M. Mowers, "Bright future: Solar power as a major contributor to the u.s. grid," *IEEE Power and Energy Mag.*, vol. 11, no. 2, pp. 22–32, March 2013.

[4] S.-T. Kim, S. Bae, Y. C. Kang, and J.-W. Park, "Energy management based on the photovoltaic hpcs with an energy storage device," *IEEE Trans. Ind. Electron.*, vol. 62, no. 7, pp. 4608–4617, July 2015.

[5] R. Dougal, S. Liu, and R. White, "Power and life extension of battery-ultracapacitor hybrids," *IEEE Trans. Compon. Packag. Technol.*, vol. 25, no. 1, pp. 120–131, Mar 2002.

[6] C. Abbey and G. Joos, "Supercapacitor energy storage for wind energy applications," *IEEE Trans. Ind. Applic.*, vol. 43, no. 3, pp. 769–776, May 2007.

[7] F. Baalbergen, P. Bauer, and J. Ferreira, "Energy storage and power management for typical 4q-load," *IEEE Trans. Ind. Electron.*, vol. 56, no. 5, pp. 1485–1498, May 2009.

[8] N. R. Tummuru, M. K. Mishra, and S. Srinivas, "Dynamic energy management of renewable grid integrated hybrid energy storage system," *IEEE Trans. Ind. Electron.*, vol. 62, no. 12, pp. 7728–7737, Dec 2015.

[9] G. Wang, M. Ciobotaru, and V. Agelidis, "Power smoothing of large solar pv plant using hybrid energy storage," *IEEE Trans. Sustain. Energy*, vol. 5, no. 3, pp. 834–842, July 2014.

[10] B. Indu Rani, G. Saravana Ilango, and C. Nagamani, "Control strategy for power flow management in a pv system supplying dc loads," *IEEE Trans. Ind. Electron.*, vol. 60, no. 8, pp. 3185–3194, Aug 2013.

[11] Y.-M. Chen, H.-C. Wu, Y.-C. Chen, K.-Y. Lee, and S.-S. Shyu, "The ac line current regulation strategy for the grid-connected pv system," *IEEE Trans. Power Electron.*, vol. 25, no. 1, pp. 209–218, Jan 2010.

[12] F. Savoye, P. Venet, M. Millet, and J. Groot, "Impact of periodic current pulses on li-ion battery performance," *IEEE Trans. Ind. Electron.*, vol. 59, no. 9, pp. 3481–3488, Sept 2012.

[13] L. Chen and S. Mei, "An integrated control and protection system for photovoltaic microgrids," *CSEE Journal of Power and Energy Systems*, vol. 1, no. 1, pp. 36–42, March 2015.

[14] D. Wang and F. Z. Peng, "Smart gateway grid: A dg-based residential electric power supply system," *IEEE Trans. Smart Grid*, vol. 3, no. 4, pp. 2232–2239, Dec 2012.

[15] M. Sechilariu, B. Wang, and F. Locment, "Building integrated photovoltaic system with energy storage and smart grid communication," *IEEE Trans. Ind. Electron.*, vol. 60, no. 4, pp. 1607–1618, April 2013.
[16] S. Lee, G. Son, and J.-W. Park, "Power management and control for grid-connected dgs with intentional islanding operation of inverter," *IEEE Trans. Power Systems*, vol. 28, no. 2, pp. 1235–1244, May 2013.
[17] M. Hosseinzadeh and F. Salmasi, "Power management of an isolated hybrid ac/dc micro-grid with fuzzy control of battery banks," *IET Renewable Power Generation*, vol. 9, no. 5, pp. 484–493, 2015.
[18] Y. K. Chen, Y. C. Wu, C. C. Song, and Y. S. Chen, "Design and implementation of energy management system with fuzzy control for dc microgrid systems," *IEEE Trans. Power Electron.*, vol. 28, no. 4, pp. 1563–1570, April 2013.
[19] S. Teleke, M. Baran, S. Bhattacharya, and A. Huang, "Rule-based control of battery energy storage for dispatching intermittent renewable sources," *IEEE Trans. Sustain. Energy.*, vol. 1, no. 3, pp. 117–124, Oct 2010.
[20] H. Kanchev, D. Lu, F. Colas, V. Lazarov, and B. Francois, "Energy management and operational planning of a microgrid with a pv-based active generator for smart grid applications," *IEEE Trans. Ind. Electron.*, vol. 58, no. 10, pp. 4583–4592, Oct 2011.
[21] H. Fakham, D. Lu, and B. Francois, "Power control design of a battery charger in a hybrid active pv generator for load-following applications," *IEEE Trans. Ind. Electron.*, vol. 58, no. 1, pp. 85–94, Jan 2011.
[22] C. Jin, P. Wang, J. Xiao, Y. Tang, and F. H. Choo, "Implementation of hierarchical control in dc microgrids," *IEEE Trans. Ind. Electron.*, vol. 61, no. 8, pp. 4032–4042, Aug 2014.
[23] D. Chen, L. Xu, and L. Yao, "Dc voltage variation based autonomous control of dc microgrids," *IEEE Trans. Power Del.*, vol. 28, no. 2, pp. 637–648, April 2013.
[24] B. Hredzak, V. Agelidis, and G. Demetriades, "A low complexity control system for a hybrid dc power source based on ultracapacitor-acid battery configuration," *IEEE Trans. Power Electron.*, vol. 29, no. 6, pp. 2882–2891, June 2014.
[25] S. I. Ganesan, D. Pattabiraman, R. K. Govindarajan, M. Rajan, and C. Nagamani, "Control scheme for a bidirectional converter in a self-sustaining low-voltage dc nanogrid," *IEEE Trans. Ind. Electron.*, vol. 62, no. 10, pp. 6317–6326, Oct 2015.
[26] B. Hredzak, V. Agelidis, and M. Jang, "A model predictive control system for a hybrid battery-ultracapacitor power source," *IEEE Trans. Power Electron.*, vol. 29, no. 3, pp. 1469–1479, March 2014.
[27] H. Liu, Z. Zabinsky, and W. Kohn, "Rule-based control system design for smart grids," in *Power and Energy Society General Meeting, 2010 IEEE*, July 2010, pp. 1–5.
[28] H. Zeineldin and J. Kirtley, "A simple technique for islanding detection with negligible nondetection zone," *IEEE Trans. Power Del.*, vol. 24, no. 2, pp. 779–786, April 2009.

Srikanth Kotra (S'15) was born in Lingala, Warangal, India in 1991. He received his Bachelor degree from Jawaharlal Nehru Technological University, Hyderabad, India, in 2012. Presently he is pursuing Ph.D. at Indian Institute of Technology Madras, Chennai, India. His research interests include power electronic converter applications in microgrid and renewable energy systems and electric vehicles.

Mr. Srikanth is the recipient of the Best Paper Award at the 2015 IEEE India Conference (INDICON) held at New Delhi, India and the Best Presentation Award at 2015 IEEE Industrial Electronics Conference (IECON) held at Yokohama, Japan.

Mahesh K. Mishra (S'00-M'02-SM'10) received the B.Tech. degree from the College of Technology, Pantnagar, India in 1991, the M.E. degree from the University of Roorkee, Roorkee, India, in 1993, and the Ph.D. degree in electrical engineering from the Indian Institute of Technology, Kanpur, India, in 2002.

He has teaching and research experience of about 20 years. For about ten years, he was with the Electrical Engineering Department, Visvesvaraya National Institute of Technology, Nagpur, India. Currently, he is a Professor in the Electrical Engineering Department, Indian Institute of Technology Madras, Chennai. His interests are in the areas of power distribution systems, power electronic applications in microgrid and renewable energy systems.

Dr. Mahesh is life member of the Indian Society of Technical Education (ISTE).